Surface Minimal Bactericidal Concentration: A comparative study of active glasses functionalized with different-sized silver nanoparticles

Surface Minimal Bactericidal Concentration: A comparative study of active glasses functionalized with different-sized silver nanoparticles

Giulia Barzan[a,b], Luca Rocchetti[c], Chiara Portesi[a], Francesco Pellegrino[c], Gianmario Martra[c], Angelo Taglietti[d], Andrea Mario Rossi[a] and Andrea Mario Giovannozzi[a*]

[a] *Quantum Metrology and Nano Technologies Division, Istituto Nazionale di Ricerca Metrologica (INRiM), Strada delle Cacce, 91, 10135 Turin, Italy;*

[b] *Departement of Electronics and Telecommunications, Politecnico di Torino, Corso Duca degli Abruzzi, 24, 10129 Turin, Italy;*

[c] *Department of Chemistry and NIS Inter-Departmental Centre, University of Torino, Via Pietro Giuria, 9, 10125 Turin, Italy*

[d] *Department of Chemistry, General Chemistry Section, University of Pavia, viale Taramelli, 12, 27100 Pavia, Italy;*

[*] *Corresponding author: Andrea Mario Giovannozzi, tel +39 011 3919330; e-mail a.giovannozzi@inrim.it*

Abstract (150-250 parole)

In this work the quantification of antimicrobial properties of differently sized colloidal AgNPs immobilized on a surface have been studied. Three different sizes of spheroidal shaped AgNPs with a diameter of 6 nm, 30 nm and 52 nm were synthetized and characterized with UV-VIS, SEM, TEM and ICP-MS. The MIC (Minimal Inhibitory Concentration) and MBC (Minimal Bactericidal Concentration) against *Escherichia coli* ATCC 8739 were investigated. Then, the antibacterial efficacy (R) of amino-silanized glasses coated with different amounts of the three sizes of AgNPs were quantified by international standard ISO 22196 adapted protocol against *E. coli*, clarifying the relationship between size and antibacterial properties of immobilized AgNPs on a surface. The total amount of silver present on glasses with an $R \sim 6$ for each AgNPs size was quantified with ICP-MS and this was considered the Surface MBC (SMBC), which were found to be 0.023, 0.026 and 0.034 $\mu g/cm^2$ for AgNPs 6, 30 and 52 nm respectively. Thus, this study demonstrate that active surfaces with a bactericidal effect at least $\geq$ 99.9999 % could be obtained using an amount of silver almost 1000 times lower than the MBC found for colloidal AgNPs. The immobilization reduces the aggregation phenomena that occur in nanoparticles suspensions and maximizes the exposed surface-area promoting direct contact with bacteria. Starting from this glass model system, our work could broaden the way to the development of a wide range of antibacterial materials with very low amount of silver that can be safely applied in many fields.

keywords: (max 6) silver nanoparticles, E. coli, antibacterial properties, surface minimum bactericidal concentration, glass silaniztion, APTES

1. Introduction

In recent years the overuse and misuse of antibiotics has led to an escalation of the global issue of the development of drug-resistant organisms. This has driven many research fields to turn their attention into valid alternatives to classical antibiotics. In this context, great interest was arisen by metallic nanoparticles. In particular, silver nanoparticles (AgNPs) were extensively studied and applied in medicine due to their lower tendencies to develop microbial resistance [1], broad spectrum killing [2] and unique plasmonic properties in the visible region [3]. Colloidal silver has already demonstrated its bactericidal and antiviral effect [4] that can be explained by damage to the cell membrane and intracellular metabolic activity [5]. However, silver in low concentrations, as 0.01 mg/m^3, is not toxic for human and animal cells [6–8] and is considered environmentally friendly, even if some concern is raised for the overall impact on health and environment. As a result, silver nanoparticles have emerged as the most widely used nano-antimicrobial in many consumer products such as cosmetics, textiles, dietary supplements, food packaging, surgical coatings, medical implants, and water disinfection applications. Due to their large surface-to-volume ratio and quantum confinement effect AgNPs exhibit different physical, chemical, and biological properties compared to bulk materials [9]. When they interact with microorganisms (bacteria, fungi, and viruses), silver ions (Ag^+) are released and these ions may affect and damage the microorganism, attacking the negatively-charged cell walls of the microbes and thus deactivating cellular enzymes, disrupting membrane permeability leading to cell lysis, or interacting with the thiol groups of enzyme and proteins that are important for the bacterial respiration [10]. Despite Ag^+ ions, AgNPs exert antimicrobial effects themselves by

anchoring and penetrating to the bacterial cell wall, interfering with cellular signalling, which is critical for cell viability and division [11,12] Several studies demonstrated that many physicochemical properties of AgNPs, such as stability, size, shape, and surface chemistry, play important roles in their antibacterial activity and modulate their interactions with microorganisms [10,13–18]. Size is normally considered a key factor in the antibacterial activity of AgNPs. A size dependent antibacterial activity was observed in several studies [13,19,20] with a gradual increase of such activity as size decreases from 100 nm to 20 nm, and with a dramatic enhancement as the size gets down at the sub-10 nm scale. Since the surface area involves the increase of contact surface, the higher microbicidal effect can be expected from smaller particles because they have a higher exposed metallic surface [21], which facilitates the adhesion to the bacteria membrane and ultimately the entrance into the cytoplasm. Smaller silver particles also release silver ions faster, leading to a higher toxicity due to a higher effective silver ion concentration [22]. In addition to size, the shape was also found to affect antibacterial activity of AgNPs. Results from Pal et al. [16], demonstrated that truncated triangular nanosilver exhibited the highest biocidal activity followed by silver nanospheres and nanorods. Since most of these antibacterial studies were conducted in liquid, AgNPs are usually exposed to various liquid environments, such as culture medium and body fluids, that affect their dispersion stability in these media with a significant change of the AgNPs' size, surface-to-volume ratio, morphology, silver-ion release kinetics, and thus the antibacterial activity [23]. Results from Kvítek et al., 2008 [24] and Radniecki et al. [25] , demonstrated how the dispersion stability and the chemical stability influence antibacterial activity of AgNPs with a significant decrease of the minimum inhibitory concentration (MIC) when a surfactant/polymer surface modifier is used in comparison with the unmodified

dispersion. However, the majority of these findings are mostly related to the interaction of AgNPs colloidal suspensions with bacteria in liquid media but very little is known on the relations between size and bactericidal properties of AgNPs when they are anchored to a surface [26]. Several studies demonstrated the antibacterial properties of different types of surfaces, such as bio/polymers [27,28], fabrics, textiles [29] or glass [30,31], coated or incorporated with AgNPs. However, to the authors' knowledge, a comparative study on the size effect and on the surface loading of the AgNPs in respect to the antibacterial properties is not present. In this work, three different size of spheroidal shape AgNPs (6 ± 3 nm, 30 ± 6 nm, 52 ± 7 nm) were produced and characterized for shape, dimensions, dispersion in liquid medium and Ag content, to calculate their exposed surface/mass ratio. MIC (Minimal Inhibitory Concentration) and MBC (Minimal Bactericidal Concentration) against the model Gram negative bacterium *Escherichia coli* ATCC 8739 were investigated in liquid to confirm the highest bactericidal effect of the smaller AgNPs. Then, all the three different size of AgNPs were anchored to a model glass surface using the ''layer-by-layer" (LbL) approach described by Pallavicini et al. [32] to obtain thin films of AgNPs deposited on a molecular self-assembled monolayer (SAM) of an amino silane. Glass slides coated with three sizes of AgNPs at a different percentage of coverage were prepared and their antibacterial property against E. coli was quantified by the international standard ISO 22196 to evaluate i) the dependence of the bactericidal effect on the AgNP size and ii) to quantify the MBC for each type of AgNPs modified surfaces. Moreover, a comparison analysis on the MBC values provided by the AgNPs in form of colloidal suspensions and anchored to solid surfaces is discussed to better elucidate the different mechanisms of action and the overall antibacterial performance in these two different configurations.

2. Material and Methods

2.1 Chemicals

Silver nitrate (>99.8%), sodium borohydride (>99.0%), sodium citrate (>99.0%) and (3-mercaptopropyl)trimethoxysilane (≥98%, APTES), Luria Barthani (LB) broth, LB agar, PBS tablets pH 7.4 (for 200 ml) and Nutrient broth (NB) components were purchased by Sigma Aldrich and all were diluted in Milli-Q water. Microscope glass slides (26 x 76 mm, 1.0-1.2 mm thick) were purchased from Aptaca.

Plate count agar (PCA) was purchased from Lickson. Soybean casein digest broth and polyoxyethylene sorbitan monooleate (SCDLP) with lecithin was prepared, polyoxyethylene sorbitan monooleate (Tween 80) was purchased by Scharlau Microbiology.

The pH of each culture medium was adjusted between 6.8 and 7.2 (at 25 °C) with NaOH and HCl 0.1 M solutions.

Phosphate-buffered physological saline (PPS) was prepared adding sodium chloride in Milli-Q water and this solution was used to dilute PBS 800 fold. All the solutions used for the bacterial analysis were autoclaved.

2.2. Colloidal Nanoparticle preparation

The synthesis of spheroidal silver nanoparticles was adapted from a previously reported preparation [33–35]. Briefly, silver nitrate was reduced by sodium borohydride under controlled condition of temperature to produce seeds with a diameter of about 4 nm which

were used as starters to the subsequent growth of larger nanoparticles based on the stepwise seeded-growth method.

2.3 Characterization of colloidal AgNPs

Absorbance spectra of colloidal AgNPs were taken with a UV-VIS spectrophotometer (Lange DR500) in the 200-1000 nm range. Milli-Q water was used as blank.

Transmission electron microscopy (TEM) images were collected with a Jeol JEM-3010 UHR instrument with a point resolution of 0.17 nm, equipped with monocrystal of LaB_6 as thermo-ionic source, using a voltage of 300 kV. A drop of colloidal sospensions of AgNPs, prepared as described, was deposited on a copper grid (3 mm) covered by a perforated carbon thin film left to air dry before the analysis. TEM images were processed with ImageJ software [36] to calculate the relative diameter and the function of distribution of the dimensions of the colloids. For this purpose, at least 200 NPs were analysed by TEM micrographs for each AgNPs size.

Finally, Thermoscientific ICP-MS ICAP-Qs model was used to quantify the Ag concentration in each of the three different sized colloidal AgNPs. The samples were previously processed by sonication of 20 minutes at 80W, filtered with a 0.2 μm nylon filter and washed three times with Milli-Q water by centrifugation. To precipitate AgNPs, different centrifugations protocols at 4°C were adopted for each size (90 min at 21000 RCF for 6 nm AgNPs, 30 min at 4500 RCF for 30 nm AgNPs and 20 min at 2500 RCF for 52 nm AgNPs). Then, 0.5 ml of the suspensions were mineralized in hot concentrated HNO_3 in order to guarantee a complete silver solubilization. The obtained solution was subsequently diluted up to 1: 10˙000 with a final nitric acid concentration of 2% v / v.

The instrument was calibrated with a standard 2% nitric acid solution prepared by diluting standard solutions for silver to 1000 mg / l and using 45Sc, 89Y, 159Tb (100 ppb) as internal standards. The calibration curve was built on six points with an angular coefficient> 0.999 and for the quantification the silver isotope 107 (107Ag) was taken into consideration. A power of 1450 W was used with an Argon flow rate of 15 l/min, an auxiliary Argon flow of 1 l/min, a nebulised flow of 0.9 l/min and a 5 ml/min of helium flow in the collision chamber

2.4 Bacterial strain and culture conditions

E. coli ATCC 8739 strain was used for the microbiological experiments with both colloidal and glass-anchored AgNPs.

For the MIC and MBC determination of colloidal AgNPs the frozen stock culture was revitalized and let grow overnight in 5 ml of LB culture at (37 ± 1) °C with agitation (150 rpm). Then, it was plated on LB agar to obtain isolated colonies and incubated overnight at (37 ± 1) °C. Using a sterile inoculating loop, bacteria from a single colony were transferred from the stock agar culture into 5 ml of LB culture medium and incubated at (37 ± 1) °C overnight with agitation (150 rpm). The optical density at 600 nm (OD_{600}) of the bacterial suspension was measured using UV-VIS spectrophotometer (Lange DR500) in the single wavelength mode. LB without bacteria inoculated was employed as a blank, and the OD_{600} was adjusted to 0.05 then let grow at least for 1.5 h until the start of the test. Then, the OD_{600} was adjusted to 0.1 to reach a bacterial concentration of about 1 x 10^8 CFU/ml in LB to use for the inoculum.

For the evaluation of the antibacterial activity of NP-coated glass slides the same procedure was adopted using NB culture medium and agar instead of LB. Then, the OD_{600} was adjusted

to 0.1 to reach a bacterial concentration of about 1 x 10^8 CFU/ml in 1/500 NB, diluted in sterile Milli-Q water, to use for the inoculum.

2.5 Antibacterial activities of colloidal AgNP

2.5.1 Cleaning and concentration of AgNPs

Before the microbiology tests, the different types of AgNPs were processed to obtain a sterile, concentrated and homogeneous suspension of each batch. They were sonicated for 20 min at 180 W and filtered with a 0.2 μm Nylon filter. Different suspensions at known concentration were prepared in Milli-Q water to obtain three calibration curves, one for each size of AgNPs, based on their extinction UV-VIS spectra. The concentrations ranges analyzed to define a linear interval of absorbance were from 0.2 μg/ml to 10 μg/ml for all the different types of AgNPs. The maximum peaks taken into consideration were 391 nm for 6 nm AgNPs, 398 nm for 30 nm AgNPs , 419 nm for 52 nm AgNPs. To precipitate AgNPs, different centrifugations protocols at 4°C were adopted for each size (90 min at 21000 RCF for AgNPs 4nm, 30 min at 4500 RCF for AgNPs 30 nm and 20 min at 2500 RCF for AgNPs 55nm). The AgNPs were washed three times with Milli-Q sterilized water and the concentration after the cleaning was measured using the calibration curves. Then the final stock concentration was adjusted to 2 mg/ml (The calibration curves built for each AgNPs size are shown in the Supplementary Informations).

2.5.2 Determination of MIC and MBC

The procedure followed to determine the MIC and the MBC was adapted from the one described by Oritiz et al. [37]. AgNPs of different size were put in different tubes within the

desired test concentrations in 15 ml of LB and sonicated at 180 W for 20 min. Different concentrations were tested for each AgNPs size: 0.65, 1.3, 2.6, 6.4, 10.4, 13, 26, 39 μg/ml for the 6 nm AgNPs; 6.05, 12.1, 24.2, 36.4, 60.5, 97, 121, 146, 182 μg/ml for the 30 nm AgNPs and 6.6, 13.2, 26.5, 66, 106 132, 158, 198 μg/ml for the 52 nm AgNPs. For each test a negative control with only LB and two positive controls were prepared by adding 10 μg/ml of $AgNO_3$ and 10 μg/ml of Triclosan, a very well-known bactericidal agent. Each tube was then inoculated to a final bacterial concentration of 1 x 10^6 CFU/ml. The tubes were vortexed and incubated horizontally at (37 ± 1)°C under agitation at 200 rpm. The OD_{600} was measured every hour for 6 hours and after 24 h. After 24 h of incubation, each concentration tested were 10-fold serial diluted in PBS and plated on LB agar in triplicate. The plates were incubated overnight at (37 ± 1)°C and the formed bacterial colonies were counted.

2.6 Solid surfaces functionalization

Microscopy glass slides were cut manually in squares of 25 x 25 mm, cleaned firstly in Acetone then in Ethanol for 10 min under sonication. They were cleaned with aqua regia (3:1 HCl 37%:HNO_3 65%) for 15 min, washed three times with ultrapure water, immersed in piranha solution (3:1 HSO_4 xx% : H_2O_2 xx%) for 30 min at 80° C and washed other three times with ultrapure water. Glasses were then soaked for 1 hour in a 3% (v/v) solution of (3-aminopropyl)triethoxysilane in methanol at room temperature. In a typical preparation 4 glass slides were prepared at the same time, i.e. reacting in the same APTES solution inside a 4-place teflon slides holder (where the slides were kept in a vertical position). After this, the amino-modified glasses were washed under sonication with methanol, dried under a nitrogen stream, moved to a 4-place glass holder and kept thermostatically at 150°C for 1 hour.

Finally, after cooling down to room temperature, they were incubated with 30 ml of colloidal AgNPs of the desired size and dilution for different times. Many dilutions of the three different sized AgNPs were analyzed to obtain glass slides with various percentages of coverage. The functionalized glasses were then washed with ultrapure water and let air dry vertically in the slides holder.

2.7 Active glass characterization

Absorbance spectra of AgNPs-functionalized glass were taken with a UV-Vis spectrophotometer (Lange DR500) in the 200-1000 nm range. Spectra were obtained placing the glasses in the apparatus equipped with a film holder, using a non-functionalized cleaned glass as blank.

Scanning electron microscopy (SEM) analysis of the glass slides was performed using a SEM FEI Inspect F in UHV. For preventing the charging of the samples, that would otherwise occur because of the accumulation of static electric field and also for increasing the amount of secondary electrons to be collected during the SEM measurement, the samples were sputter coated with 10 nm of Au film. An acceleration potential of 10 kV, with a spot of 3.5 and a magnification of 10000X were used to acquire at least five images in different zones of the samples, in order to get the estimation of the average distribution of the nanoparticles on the glass surface. The images were analyzed with ImageJ and converted to binary to obtain the percentage of area covered by silver nanoparticles.

Quantification of Ag coverage on glass was performed on three selected functionalized glasses in duplicate, two for each AgNPs size. The glasses were chosen among the first AgNPs dilution that demonstrated to kill *E. coli* (this was considered the MBC for the

anchored AgNPs) for each of the three different nanoparticle sizes. Two glass slides without AgNPs, functionalized only with APTES, were analyzed as negative controls. AgNPs were detached from glasses by soaking the slides in nitric acid 65% for 3 hours and sonicated for 2 minutes, then the final volume was brought to 25 ml with nitric acid. The samples were then treated in microwave (30 min at 150°C) to dissolve the residual AgNPs and finally diluted to obtain a nitric acid concentration of 5%.

The solutions were analyzed with an ICP-MS apparatus in order to quantify the Ag. ICP-MS analyses were carried out using a Thermoscientific ICP-MS ICAP-Qs model, equipped with a quadrupole mass analyzer and a flatpole quadrupole collision / reaction cell. The instrument is calibrated with 5% standard nitric acid standard for Ag prepared by diluting standard reference certificates at 1000 mg l-1 using ^{45}Sc, ^{89}Y, ^{159}Tb (100 ppb) as internal standards. The calibration curve was constructed with 7 points (100, 50, 25, 10, 5, 1 and 0.3 ppb) and linear correlation coefficient > 0.999. Interference due to polyatomic ions is eliminated by operating the collision cell in He mode with kinetic energy discrimination (He - KED). ^{107}Ag was used for quantitation. Other parameters as follows: RF power 1450 W; Main Ar Flow 15 L min^{1}; Ar auxiliary flow 1.0 L min^{-1}; Nebulizer flow 0.90 L min^{-1}; Concentric nebulizer with impact sphere; Collision cell He flow 5.0 mL min^{-1}.Extraction Lens voltages and KED bias auto-optimized with the tuning solution suggested by the vendor.

2.8 Antibacterial activities of AgNPs-modified glass slides

The followed procedure was adapted from the ISO 22196:2011 [38]. Three AgNPs-functionalized glass slides (25 x 25 mm) of each test and six untreated samples (glass without AgNPs coating) were sterilized in Ethanol 70% for 20 min. Then, all samples were placed in

Petri dishes with the active surface up and inoculated with 100 µl of the prepared *E. coli* suspension to obtain $1x10^6$ CFU/ml on each glass and covered with 20 x 20 mm pieces of sterile films obtained from autoclavable plastic bags with a thickness of 50 µm.

Half of the untreated glass was used for the determination of the initial cell count directly after inoculation.

After incubation for 5 h at (35 ±1)°C under relative humidity of not less than 90 %, the bacteria were harvested from the glass surfaces of the three test samples and the remaining three untreated subsamples, using 10 ml of SCDLP broth and agitated gently at 90 rpm for 10 min. Then the SCDLP was collected from the Petri dish, serially diluted in PPS and plated by inclusion in 15 ml of PCA .

After 24 h at (35 ± 1) °C the plates were counted and antimicrobial activity was expressed as the R value. The R value, which is the decimal-log reduction rate, was calculated.

3. Results and discussion

3.1 Characterization of different sized colloidal AgNPs

Three different sizes of citrate-capped spheroidal shaped AgNPs with a nominal diameter of 6 nm, 30 nm and 52 nm were produced by a *stepwise seeded growth* synthesis method, as described in paragraph 2.2, and characterized with different analytical techniques. Firstly, their shape and dimensions were determined with TEM (Fig. 1 a-b-c), while their optical properties and agglomeration state with UV-Vis spectroscopy (Fig. 1 d-e-f); then, a quantitative analysis on the total Ag in solution for every type of AgNPs was performed with

ICP-MS. The characteristics of the three different sized silver nanoparticles and the calculated specific superface area and number of AgNPs/ml are summarized in Table S1.

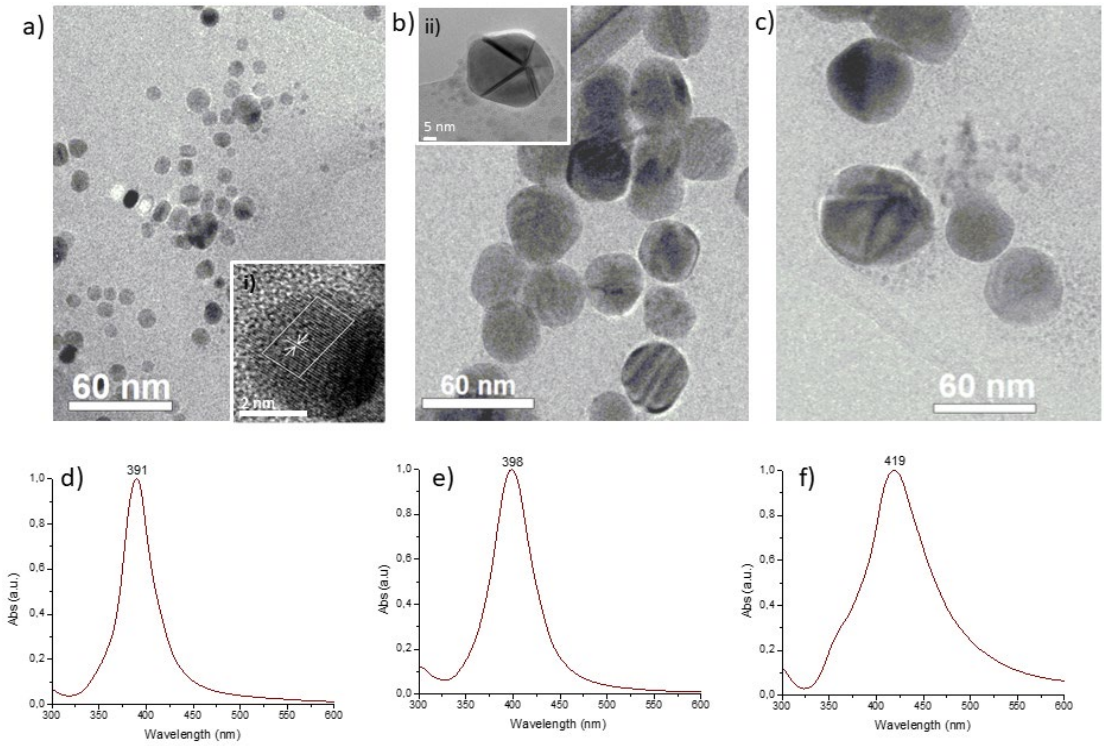

Fig. 1 TEM and UV-Vis colloidal AgNPs characterization: a-b-c) TEM images of colloidal AgNPs 6 nm, 30 nm and 52 nm respectively. Inset i) Highly resolute TEM image that shows the lattice fringe of a 6 nm nanoparticle. Inset ii) TEM image that shows a particular pyramidal shape of a 30 nm nanoparticle. **d-e-f)** UV-vis absorbance spectra of colloidal AgNPs 6 nm, 30 nm and 52 nm from left to right respectively, with the reference maximum absorbance peaks which are respectively: 391 nm, 398 nm and 419 nm.

TEM analysis revealed a spheroidal shape for all the synthesized AgNPs with the expected average diameters of 6, 30 and 52 nm (Fig. 1 a-c). TEM was also used to evaluate the crystallinity degree of the different AgNPs samples. As the inset i of Fig.1 shows, the distance

between two crystallinity planes was measured as 2,4 Å for all the three samples, which is in accordance to data on single crystalline silver nanoparticles reported in literature [39], this *d-spacing* of lattice fringes corresponds to the (200) plane of silver. In case of AgNPs growth from seeds, i.e. AgNPs of 30 and 52 nm, HRTEM images showed the presence of multiple-twinned crystalline planes. In particular, the inset in Fig.1b ii shows a five-fold multiple twinned decahedron crystal, which is favored for fcc growth of silver. The presence of multiple twinned particles normally indicates that silver nuclei/particles formed at the first stage undergo Ostwald ripening in the second stage and are transformed into larger silver nanoparticles, thus completing the growth process [13,40].

The UV-VIS extinction spectra can also provide information about the size, shape, size distribution and the agglomeration state of the synthetized AgNPs. As Fig. 1 d-e-f shows, the λ_{max} of the AgNPs UV-VIS spectra increases from 391 nm to 417 nm, showing a red-shift of the Local Surface Plasmon Resonance (LSPR) peak as the relative particle size increase from 6 to 52 nm [41]. Single, narrow and symmetric absorption peaks attests a good homogeneity in terms of size distribution and spheroidal shape which also was confirmed by TEM analysis. The full width half maximum (FWHM) of the LSPR peaks, which can also be related to the dispersion of the nanoparticles dimensions, tends to increase with the size of the AgNPs due to the increase of the scattering and to the occurring of quadrupole resonance modes.

The concentration of silver in each type of AgNPs stock was determined through ICP-MS analyses and the results are collected in table 1. This allowed the setup of specific calibration curves for each AgNPs size based on the UV-VIS extinction spectra. A linear trend was calculated between the silver concentration and the λ_{max} absorbance peak for each AgNPs size in the range of 0 -10 µg/ml (Fig. S1).

A summary of the physiochemical properties of the synthetized AgNPs, such as shape, size distribution, surface area and number of NPs, is reported in the Supplementary (Table S1).

3.2 MIC and MBC determination of colloidal AgNPs

MIC (minimum inhibitory concentration) and MBC (minimum bactericidal concentration) of the three differently sized colloidal AgNPs towards *E. coli* ATCC 8739 were investigated performing both broth dilution method (BDM) and CFU assay, as described by the National Committee for Control of Laboratory Standards (NCCLS) guide lines [42]. A previous work by Agnihotri et al. [13] on a similar *E. coli* strain reported a MIC of Ag (µg/ml) around 50, 90 and 110 µg/ml for AgNPs with a diameter size of 5, 30 and 50 nm, respectively. Therefore, different NPs concentrations were tested depending on the AgNPs size. In particular, a concentration range from 0.65 µg/ml to 39 µg/ml was chosen for 6 nm AgNPs (Fig. 2 a i), 6.05 µg/ml to 182 µg/ml for 30 nm AgNPs (Fig. 2 a ii) and 6.6 µg/ml to 198 µg/ml (Fig. 2 a iii) for 52 nm AgNPs.

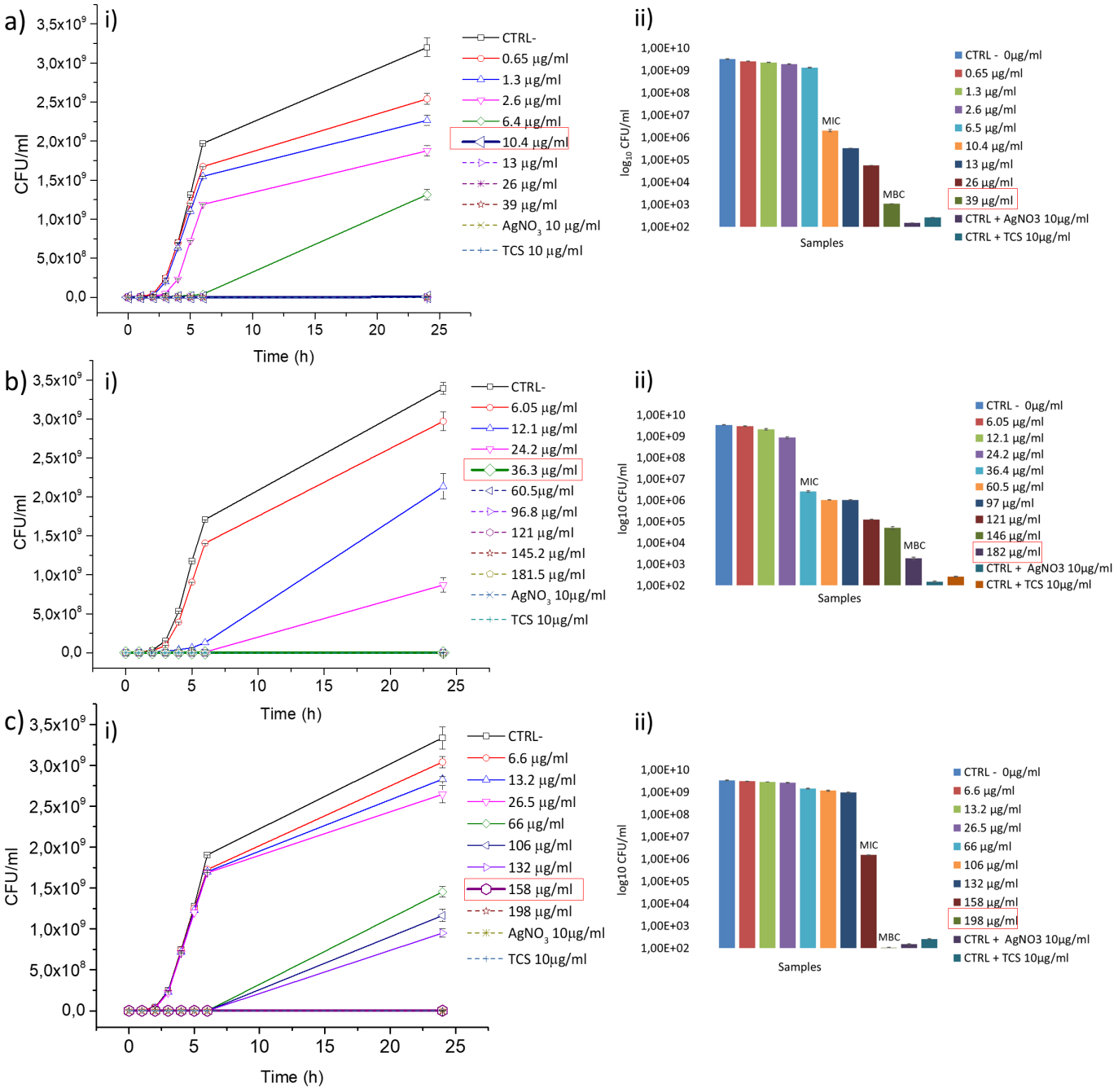

Fig. 2 MIC and MBC determination of AgNPs towards *E. coli* ATCC 8739

a) (i) BMD (broth microdilution) test results to investigate the MIC of AgNPs 6 nm against *E. coli* ATCC 8739. UV-Vis measurements were taken over 24 h then the CFU/ml were calculated from the OD_{600} and plotted against time. 10 µg/ml of TCS and $AgNO_3$ were used

as positive controls. (ii) Histogram of the *E. coli* ATCC 8739 CFU enumeration performed for the MBC analyses. The AgNPs concentrations investigated and the controls were same used for the MIC. **b)** (i) BMD test results to investigate the MIC of AgNPs 30 nm against *E. coli* ATCC 8739. (ii) Histogram of the *E. coli* ATCC 8739 CFU enumeration performed for the MBC analyses. **c)** (i) BMD test results to investigate the MIC of AgNPs 52 nm against *E. coli* ATCC 8739. (ii) Histogram of the *E. coli* ATCC 8739 CFU enumeration performed for the MBC analyses.

As Fig. 2 shows, the MIC value for 6 nm AgNPs toward *E. coli* resulted to be 10.4 µg/ml (Fig. 3a i). Treating bacteria with this AgNPs concentration resulted in a bacterial growth after 24h of 2 x 10^6 CFU/ml, corresponding to the start inoculum. For the same sample the count of vital cells after 24h of treatment identified an MBC of 39 µg/ml (Fig. 2b i). At this concentration a decrease of the value of CFU/ml, which corresponds to a bacterial killing of 99.99% was obtained. The 30nm AgNPs showed a MIC of 36.4 µg/ml (Fig. 2a ii) with a bacterial growth of 2.5 CFU/ml after 24h, and an MBC of 182 µg/ml (Fig. 2b ii), while the AgNPs 52 nm exhibited a MIC of 158 µg/ml (Fig. 2a iii) and an MBC of 198 µg/ml (Fig. 2b iii). These results are in good agreement with the already published data of AgNPs of comparable sizes and further confirmed the highest antibacterial effect of smaller AgNPs (size below 10 nm) based on the reported MIC and MBC values. This is particularly evident in the plot of Fig.3a, where the calculated killing trend of E. coli after 24h exposure to AgNPs mainly depends on their size, with a higher killing efficiency at lower concentrations by the 6 nm AgNPs followed by 30 and 52 nm AgNPs.

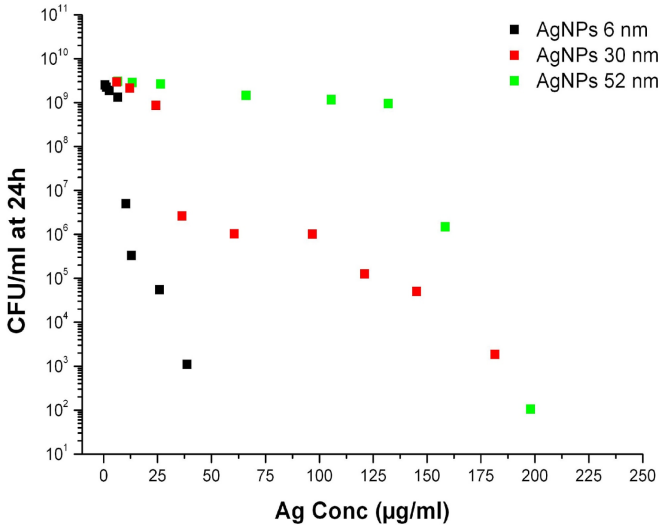

Fig. 3 : Comparison of the three colloidal AgNPs sizes antibacterial effects with respect to the silver concentration.

Plot of the CFU/ml counted after 24h of incubation of *E. coli* with the colloidal AgNPs 6 nm (black squares), 30 nm (red squares) and 52 nm (green squares) *vs* the silver concentration of each sample (which are the ones used for the MIC and MBC experiments).

Table 1: Bactericidal properties characterization of AgNPs colloidal suspensions

AgNPs nominal size (nm)	MIC (µg/ml)	Number of AgNPs at the MIC (NPS/ml)	Surface Area AgNPs at the MIC (nm^2/ml)	MBC (µg/ml)	Number of AgNPs at the MBC (NPs/ml)	Surface Area AgNPs at the MBC (nm^2/ml)
6	10.4	8.67×10^{12}	9.80×10^{14}	39	3.25×10^{13}	3.68×10^{15}
30	36.4	2.45×10^{11}	6.92×10^{14}	182	1.22×10^{12}	3.46×10^{15}
52	158	1.94×10^{11}	1.7×10^{15}	198	2.42×10^{11}	2.14×10^{15}

Then, to better understand the bactericidal action mechanism of different sized AgNPs, their aggregation state was studied by monitoring the profile of the UV-VIS spectra at different

concentrations of AgNPs both in water and in LB broth (Fig S2). These studies revealed that the aggregation phenomenon is really evident in the culture medium in respect to the water and it increases proportionally with the size and the concentration of the nanoparticles, as indicated by the formation of broad plasmonic bands in the spectral region between 450-800 nm. This suggests that the killing efficiency associated to smaller NPs and promoted by their higher specific surface area is probably reduced due to their agglomeration, while bigger AgNPs displayed a comparable bactericidal effect due to their higher silver content. It could be assumed that above a certain concentration value even the smallest AgNPs are no longer capable to penetrate bacterial cells because they are stuck together. Consequently, with the formation of agglomerate that become bigger with the increase of the AgNPs concentration in liquid, the exposed surface areas become nearly the same for each of the three sizes so the dominant antibacterial effect could be mainly attributed to Ag^+ ions release and direct contact, losing the differences related to the size.

The stability of AgNPs in solution is, in fact, a big issue for their applications and it was very debated in literature, since the generation of spacious aggregates often leads to a loss of the antibacterial activity [11,43]. To avoid this problem many groups found different methods to stabilize them in solution by adding polymers or surfactant in the colloidal suspension [24], or by coating their surface with glutathione (GSH) [21] or with polyethylene glycol (PEG) [44]. However, in this work, in order to study the bactericidal activity of the AgNPs in respect to their size, they were anchored on a solid surface as monolayers to avoid their aggregation and to compare their bactericidal effect with the results obtained in liquid.

3. 3 Preparation and characterization of AgNPs-modified glass substrates

Glass silanization with amino-functional moieties is a well-established method to anchor metallic NPs on the glass surface. This method mainly exploits the electrostatic interaction between the positively charged amino groups with the negatively charged carboxylic moieties of the citrate capped AgNPs to obtain a stable and dense monolayer of NPs on the glass substrate [26,31] Different levels of AgNPs surface coverage is usually obtained by changing NPs concentration and/or the incubation time. UV-VIS analysis together with SEM were first performed to study the attachment of the different types of AgNPs on glass and to evaluate the surface coverage over time.

As example, Fig. 4 shows SEM and UV-VIS characterization of four glass substrates incubated for different times with the 52 nm AgNPs .

As the incubation time of the AgNPs on glass is increased from 1h to ON, the colour of the slides moves from a light yellow to dark yellow, indicating a higher level of surface coverage (Fig.4a). This is indeed confirmed by the UV-VIS spectra in Fig.4b where a progressive increase of the intensity of the extinction is observed over time. The UV-VIS spectra (Fig. 4b) showed that, in comparison with the colloidal suspension, the typical LSPR peak of the 52 nm AgNPs shifted towards shorter wavelength from 419 to 395 nm due to a change of the refractive index surrounding NPs, i.e. from water to air. This phenomenon is very well known and already documented in previous works [26,31]. Moreover, as soon as the incubation time is increased, a broad band centered at 600-800 nm showed up, which is related to the plasmonic coupling of AgNPs in close proximity and to the formation of aggregates on the surface. A similar behavior was also observed in the samples covered with the 6 and 30 nm AgNPs (Fig.S3), where, in addition to the expected and increasing LSPR peaks close to 400 nm, new absorptions around 500 (for 6 nm AgNPs) and 650 (for 30 nm) nm appeared and

increased with deposition time. SEM analysis (Fig.4c) further confirms the progressive surface coverage of AgNPs over time. In particular, at lower incubation times (1 and 2h), all nanoparticles are present in a well-segregated manner with only few nanoclusters of three to six NPs on the surface, thus confirming the single LSPR peak in the extinction spectra at the corresponding times.

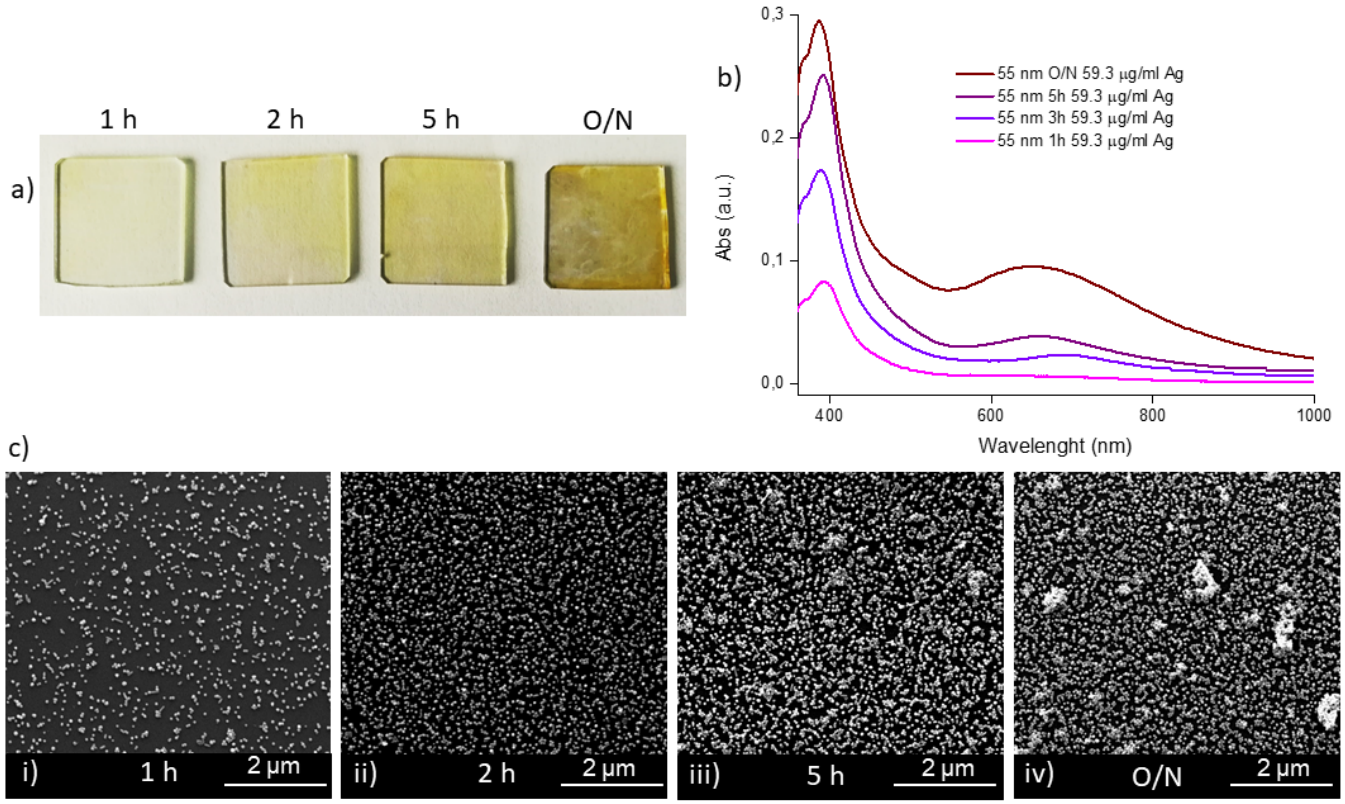

Fig. 4 UV-vis and SEM characterization of AgNPs functionalized glass slides

a) Images of APTES functionalized glass slides incubated with AgNPs 55 nm at a concentration of 59.3 µg/ml for four different time spans (1h, 3h, 5h O/N from left to right respectively) **b)** UV-VIS absorbance spectra of the four AgNPs functionalized glasses described in a **c)** SEM images of the glass slides described in a.

The deposition protocols were optimized for each size of AgNPs by changing the incubation time in order to find the optimal conditions to produce a homogeneous and stable monolayer together with a maximized surface coverage. The highest coverage rate was calculated from SEM images of 30 and 52 nm AgNPs covered glasses using ImageJ software, as described in paragraph 2.7 (Fig. S4), and it was around 25-30 % for both the two sizes. Comparing SEM with UV-VIS analysis it was observed that the optimal surface coverage for 30 nm AgNPs was obtained after 30 min of incubation, while longer deposition times are required for 52 nm AgNPs reaching a satisfying coverage after 1 hour. Longer deposition times only increase the formation of aggregates on the surface without really changing the surface coverage. As far as the 6 nm AgNPs are concerned, since SEM images were not useful due the low resolution of the technique for this size of AgNPs, the evaluation of the surface coverage rate was only conducted by UV-VIS analysis. It was observed that for smaller AgNPs a lower incubation time is required to reach the highest surface coverage. UV-VIS characterization showed that 6 nm AgNPs reached the maximum coverage rate already after 15 minutes, since the UV-VIS spectra were almost overlapped for longer time spans (Fig. S3 a).

3. 4 Antibacterial characterization of AgNPs functionalized glass substrates

The bactericidal efficacy of glasses obtained with the above mentioned optimized protocols was tested for each AgNPs size using the ISO 22196 procedure, leaving bacteria in contact with the samples for 24 hours. All these tested substrates reached a bacterial killing rate of 99,9999% with no bacterial colony present on the agar plate, thus resulting in R values ≥ 5. The R value corresponds to the decimal log reduction rate of viable bacteria, so a surface that reaches an $R > 4$ is considered an optimum antibacterial material. The same results were

obtained at shorter contact time with bacteria (5h) with almost no counting colonies on the plates, still demonstrating the high killing rate of these substrates. So, in order to study the antibacterial effect based on the AgNPs size and to establish the Surface MBC value for each type of active substrate, a wide range of glasses with a different surface coverage were prepared by progressively diluting the concentration of the starting AgNPs suspensions and by testing different deposition times (Fig. 5). As Fig.4 shows, the amount of AgNPs deposited on the surfaces was evaluated by UV-VIS characterization (Fig.5a i-iii), while the ISO 22196 procedure was used to quantify the antibacterial properties applying a bacteria-surface contact time of 5h (Fig.5b i-iii) using the formula:

$$R = (U_t - U_0) - (A_t - U_0) = U_t - A_t.$$

U_t is the average of the common logarithm of the number of viable bacteria, in cells/cm^2, recovered from the untreated test specimens after 5 h; U_0 is the average of the common logarithm of the number of viable bacteria, in cells/cm^2, recovered from the untreated test specimens immediately after inoculation; A_t is the average of the common logarithm of the number of viable bacteria, in cells/cm^2, recovered from the treated test specimens after 5 h. The R value can be considered as the decimal-logarithmic reduction rate. From the graphs reported in Fig. 5 it is evident that the antibacterial efficacy is proportional with the AgNPs coverage, with an increasing trend between the extinction intensity of the UV-VIS spectra and the R value. When a certain value of AgNPs coverage is obtained, the R value reaches its maximum around 5.9 and do not rise any further, this represents a percentage of bacterial killing $\geq$ 99.9999 %. The first set of samples with an optimized time of incubation that reached an R value close to 6 were identified for each type of AgNPs. These samples are indicated within the red squares and circles in Fig.5a-b i-iii and they are the one incubated for

15 min with 7.5 µg/ml of 6 nm AgNPs (R = 5.8), the one incubated for 30 min with 17 µg/ml of 30 nm AgNPs (R = 5.9) and the one incubated for 1 hour with 60 µg/ml of 52 nm AgNPs (R=5.8).

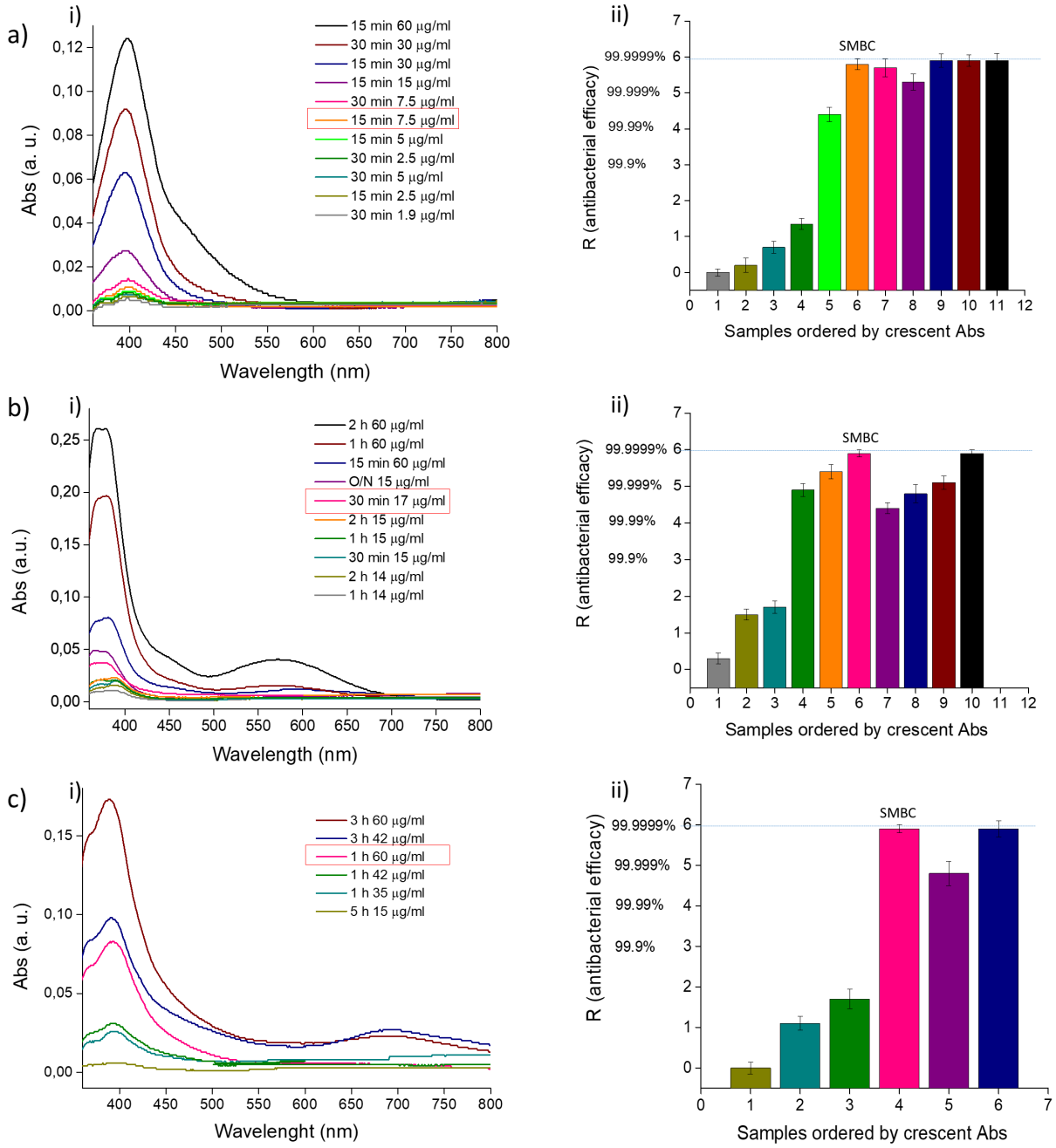

Fig. 5 UV-VIS and antibacterial characterization of AgNPs functionalized glass slides

a) (i) UV-VIS extinction spectra of glass slides functionalized with different concentration of AgNPs 6 nm incubated for different time spans (from 15 min to 30 min) (ii) Graphical representation of calculated R values of glasses analyzed in (a) ordered by crescent absorbance. **b)** (i) UV-VIS extinction spectra of glass slides functionalized with different concentration of AgNPs 30 nm incubated for different time spans (from 15 min to O/N) (ii) Graphical representation of calculated R values of glasses analyzed in (b) ordered by crescent absorbance. **c**) (i) UV-VIS extinction spectra of glass slides functionalized with different concentration of AgNPs 52 nm incubated for different time spans (from 1h to 3h) (ii) Graphical representation of calculated R values of glasses analyzed in (c) ordered by crescent absorbance.

These selected samples were analyzed with ICP-MS to quantify the amount of silver on each surface, which was calculated to be 0.023 ± 0.004 μg/cm^2 for 6 nm AgNPs, 0.026 ± 0.002 μg/cm^2 for 30nm AgNPs and 0.034 ± 0.007 μg/cm^2 for 52 nm AgNPs, respectively. If only the area exposed to bacteria is considered (4 cm^2), the total amount of silver in contact with 1 x 10^6 CFU of *E. coli* is 0.092 μg for 6 nm AgNPs, 0.104 μg for 30 nm AgNPs and 0.136 μg for 52 nm AgNPs. Such values can be considered as the Surface MBC (SMBC) for each size of immobilized AgNPs. It is interesting to notice how similar AgNPs-modified glasses proposed by Pallavicini et al., [32,45] showed a comparable antibacterial efficacy against *E. coli* ATCC 10356 using an amount of silver at least fifteen times higher than the SMBC reported in this work for 6 nm AgNPs. Thus, the calculation of the SMBC is fundamental to reduce the amount of silver needed to obtain a good antibacterial efficacy, keeping this amount to its minimum.

Moreover, in order to provide a comparison with the antibacterial tests performed on the colloidal suspensions of AgNPs, the MBC values reported in Fig.2b were converted in the absolute amount of silver (µg) exposed to 1 x 10^6 CFU of *E. coli*. All these results are summarized in Table 2.

Table 2: ICP-MS calculation of anchored AgNPs MBC

AgNPs size (nm)	MBC (µg)	Number of AgNPs at the MBC	Surface Area AgNPs at the MBC (nm^2)	SMBC (µg)	Number of AgNPs at the SMBC	Surface Area AgNPs at the Surface MBC (nm^2)
6 ± 3	39	3.25 x 10^{13}	3.68 x 10^{15}	0.092	7.73 x 10^{10}	8.74 x 10^{12}
30 ± 6	182	1.22 x 10^{12}	3.46 x 10^{15}	0.104	7.02 x 10^{8}	1.98 x 10^{12}
52 ± 7	198	2.42 x 10^{11}	2.14 x 10^{15}	0.136	1.66 x 10^{8}	1.47 x 10^{12}

As far as the silver amount on the different types of AgNPs-modified glasses is considered, a greater bactericidal effect is observed with smaller AgNPs and it progressively decrease with the increasing of the size, which is still in accordance with the antibacterial results obtained with colloidal AgNPs. However, the ratio of the MBC values reported for each type of antibacterial test, i.e. AgNPs in liquid and anchored to the surface, is quite different. In case of the antibacterial test in liquid for example, the MBC value for the 6 nm AgNPs is almost four and five times lower than the ones reported for 30 nm and 52 nm AgNPs, respectively, while this difference is greatly reduced when the AgNPs are anchored to the surface. In fact, the difference among the SMBC values registered on the AgNPs-modified glasses is only statistically significant (p value < 0.05) in respect to the 52 nm AgNPs, while no significant difference was registered between 6 nm and 30 nm AgNPs. This could be due to the reduced penetration ability inside the bacteria by smaller NPs once they are attached to the surface,

even if the number of 6 nm AgNPs and their exposed surface area, is higher than the 30 nm and 52 nm AgNPs (Table 3).

Moreover, if the MBC values of these two sets of experiments are compared, the SMBC are almost two to three orders of magnitude lower than the corresponding values in liquid. These results suggest that the immobilization of the AgNPs on the surface greatly enhances their bactericidal effects by preventing their aggregation and maximizing their contact with the bacterial cells. This was indeed previously demonstrated by Aghinotri group where citrate capped 8.6 ± 1.2 nm AgNPs displayed higher bactericidal properties when they were anchored on glass in respect to the same size in form of colloidal suspension [26]. Therefore, it can be assumed that among all possible bactericidal mechanisms of action the direct contact of AgNPs with bacteria is the one that plays the most important role in their killing efficiency.

4. Conclusions

Three differently sized spheroidal AgNPs with a diameter of 6 nm, 30 nm and 52 nm were synthetized, characterized and successfully anchored on amino-silanized glass surfaces. Then, the antibacterial activity against *E. coli* ATCC 8739 was analysed both for colloidal and immobilized AgNPs and, for the first time, a Surface Minimal Bactericidal Concentration (SMBC) was determined for each of the three sizes. In particular, the antibacterial efficacy of a wide range of amino-silanized glasses modified with different concentrations of AgNPs of each size were quantified by the international standard ISO 22196 adapted method. The lowest amount of silver found on AgNPs modified glasses that demonstrated an R∼6 (killing rate ≥ 99.9999 %) for each NPs size was quantified by ICP-MS. These values were considered the SMBC and were respectively 0.023 μg/cm^2, 0.026 μg/cm^2 and 0.034 μg/cm^2

for AgNPs 6, 30 and 52 nm. These values demonstrated to be significantly lower in respect to comparable AgNPs modified glass systems, highlighting the importance of the evaluation of the SMBC in order to minimize the quantity of silver on the surface.

Moreover, the antibacterial efficacy of the anchored AgNPs in respect to the colloidal suspensions resulted to be greatly enhanced, probably due. to the reduction of the aggregation phenomena, normally occuring in liquid media, which maximizes the exposed specific superficial area of the AgNPs as well as Ag^+ ions release and the direct contact with bacterial cells. Furthermore, the differences between the sizes resulted significantly reduced when they are immobilized on a surface, which might be desirably to reduce cytotoxicity related to small NPs [46].

Since this study is based on international standard procedure, which facilitates the comparison of the antibacterial properties of different non-porous surfaces and allows to define the minimal concentration of a specific biocide to obtain a bacterial killing $\geq$ 99.9999 %, the calculation of the SMBC could then be extended on a variety of new active materials in many fields in order to reduce the costs of production and their toxicity to a minimum.

Acknowledgements

Part of this work was carried out in collaboration with the University of Pavia. We thank Lavinia Rita Doveri for her advice about the glass coverage protocols and characterization techniques.

This research did not receive any specific grant from funding agencies in the public, commercial, or not-for-profit sectors.

References

[1] J.S. Kim, E. Kuk, K.N. Yu, J.H. Kim, S.J. Park, H.J. Lee, S.H. Kim, Y.K. Park, Y.H. Park, C.Y. Hwang, Y.K. Kim, Y.S. Lee, D.H. Jeong, M.H. Cho, Antimicrobial effects of silver nanoparticles, Nanomedicine Nanotechnology, Biol. Med. 3 (2007) 95–101. https://doi.org/10.1016/j.nano.2006.12.001.

[2] Z. Huang, X. Jiang, D. Guo, N. Gu, Controllable synthesis and biomedical applications of silver nanomaterials, J. Nanosci. Nanotechnol. 11 (2011) 9395–9408. https://doi.org/10.1166/jnn.2011.5317.

[3] G. P., G. C., S. X., Z. Q., L. S.S., T. C., C. Y., C.-P. M.B., C. M.W., W. K., X. R., P. Gunawan, C. Guan, X. Song, Q. Zhang, S.S. Leong, C. Tang, Y. Chen, M.B. Chan-Park, M.W. Chang, K. Wang, R. Xu, Hollow fiber membrane decorated with Ag/MWNTs: toward effective water disinfection and biofouling control, ACS Nano. 5 (2011) 10033–10040. https://doi.org/10.1021/nn2038725; 10.1021/nn2038725.

[4] W.R. Li, X.B. Xie, Q.S. Shi, H.Y. Zeng, Y.S. Ou-Yang, Y. Ben Chen, Antibacterial activity and mechanism of silver nanoparticles on Escherichia coli, Appl. Microbiol. Biotechnol. 85 (2010) 1115–1122. https://doi.org/10.1007/s00253-009-2159-5.

[5] S. Chernousova, M. Epple, Silver as antibacterial agent: Ion, nanoparticle, and metal, Angew. Chemie - Int. Ed. 52 (2013) 1636–1653. https://doi.org/10.1002/anie.201205923.

[6] G. Zhao, S.E. Stevens, Multiple parameters for the comprehensive evaluation of the susceptibility of Escherichia coli to the silver ion, BioMetals. 11 (1998) 27–32. https://doi.org/10.1023/A:1009253223055.

[7] P.L. Drake, K.J. Hazelwood, Exposure-related health effects of silver and silver compounds: A review, Ann. Occup. Hyg. (2005). https://doi.org/10.1093/annhyg/mei019.

[8] K. Mijnendonckx, N. Leys, J. Mahillon, S. Silver, R. Van Houdt, Antimicrobial silver: Uses, toxicity and potential for resistance, BioMetals. (2013). https://doi.org/10.1007/s10534-013-9645-z.

[9] K.H. Cho, J.E. Park, T. Osaka, S.G. Park, The study of antimicrobial activity and preservative effects of nanosilver ingredient, in: Electrochim. Acta, 2005: pp. 956–960. https://doi.org/10.1016/j.electacta.2005.04.071.

[10] B. Sadeghi, F.S. Garmaroudi, M. Hashemi, H.R. Nezhad, A. Nasrollahi, S. Ardalan, S. Ardalan, Comparison of the anti-bacterial activity on the nanosilver shapes: Nanoparticles, nanorods and nanoplates, Adv. Powder Technol. 23 (2012) 22–26. https://doi.org/10.1016/j.apt.2010.11.011.

[11] S. Shrivastava, T. Bera, A. Roy, G. Singh, P. Ramachandrarao, D. Dash, Characterization of enhanced antibacterial effects of novel silver nanoparticles, Nanotechnology. 18 (2007). https://doi.org/10.1088/0957-4484/18/22/225103.

[12] P. Pallavicini, G. Dacarro, A. Taglietti, Self-Assembled Monolayers of Silver Nanoparticles: From Intrinsic to Switchable Inorganic Antibacterial Surfaces, Eur. J.

Inorg. Chem. (2018). https://doi.org/10.1002/ejic.201800709.

[13] S. Agnihotri, S. Mukherji, S. Mukherji, Size-controlled silver nanoparticles synthesized over the range 5-100 nm using the same protocol and their antibacterial efficacy, RSC Adv. 4 (2014) 3974–3983. https://doi.org/10.1039/c3ra44507k.

[14] J. Helmlinger, C. Sengstock, C. Groß-Heitfeld, C. Mayer, T.A. Schildhauer, M. Köller, M. Epple, Silver nanoparticles with different size and shape: Equal cytotoxicity, but different antibacterial effects, RSC Adv. 6 (2016) 18490–18501. https://doi.org/10.1039/c5ra27836h.

[15] G.A. Martínez-Castañón, N. Niño-Martínez, F. Martínez-Gutierrez, J.R. Martínez-Mendoza, F. Ruiz, Synthesis and antibacterial activity of silver nanoparticles with different sizes, J. Nanoparticle Res. 10 (2008) 1343–1348. https://doi.org/10.1007/s11051-008-9428-6.

[16] S. Pal, Y.K. Tak, J.M. Song, Does the antibacterial activity of silver nanoparticles depend on the shape of the nanoparticle? A study of the gram-negative bacterium Escherichia coli, Appl. Environ. Microbiol. 73 (2007) 1712–1720. https://doi.org/10.1128/AEM.02218-06.

[17] M.A. Raza, Z. Kanwal, A. Rauf, A.N. Sabri, S. Riaz, S. Naseem, Size- and shape-dependent antibacterial studies of silver nanoparticles synthesized by wet chemical routes, Nanomaterials. 6 (2016). https://doi.org/10.3390/nano6040074.

[18] S. Tang, J. Zheng, Antibacterial Activity of Silver Nanoparticles: Structural Effects, Adv. Healthc. Mater. (2018). https://doi.org/10.1002/adhm.201701503.

[19] C.N. Baker, S.A. Stocker, D.H. Culver, C. Thornsberry, Comparison of the E test to agar dilution, broth microdilution, and agar diffusion susceptibility testing techniques by using a special challenge set of bacteria, J. Clin. Microbiol. 29 (1991) 533–538.

[20] J.R. Morones, J.L. Elechiguerra, A. Camacho, K. Holt, J.B. Kouri, J.T. Ramírez, M.J. Yacaman, The bactericidal effect of silver nanoparticles, Nanotechnology. 16 (2005) 2346–2353. https://doi.org/10.1088/0957-4484/16/10/059.

[21] E. Amato, Y.A. Diaz-Fernandez, A. Taglietti, P. Pallavicini, L. Pasotti, L. Cucca, C. Milanese, P. Grisoli, C. Dacarro, J.M. Fernandez-Hechavarria, V. Necchi, Synthesis, characterization and antibacterial activity against gram positive and gram negative bacteria of biomimetically coated silver nanoparticles, Langmuir. 27 (2011) 9165–9173. https://doi.org/10.1021/la201200r.

[22] G.A. Sotiriou, S.E. Pratsinis, Engineering nanosilver as an antibacterial, biosensor and bioimaging material, Curr. Opin. Chem. Eng. 1 (2011) 3–10. https://doi.org/10.1016/j.coche.2011.07.001.

[23] X. Yang, A.P. Gondikas, S.M. Marinakos, M. Auffan, J. Liu, H. Hsu-Kim, J.N. Meyer, Mechanism of silver nanoparticle toxicity is dependent on dissolved silver and surface coating in caenorhabditis elegans, Environ. Sci. Technol. (2012). https://doi.org/10.1021/es202417t.

[24] L. Kvítek, A. Panáček, J. Soukupová, M. Kolář, R. Večeřová, R. Prucek, M. Holecová, R. Zbořil, Effect of surfactants and polymers on stability and antibacterial activity of silver nanoparticles (NPs), J. Phys. Chem. C. 112 (2008) 5825–5834.

https://doi.org/10.1021/jp711616v.

[25] A.K. Ostermeyer, C. Kostigen Mumuper, L. Semprini, T. Radniecki, Influence of bovine serum albumin and alginate on silver nanoparticle dissolution and toxicity to Nitrosomonas europaea, Environ. Sci. Technol. (2013). https://doi.org/10.1021/es4033106.

[26] S. Agnihotri, S. Mukherji, S. Mukherji, Immobilized silver nanoparticles enhance contact killing and show highest efficacy: Elucidation of the mechanism of bactericidal action of silver, Nanoscale. (2013). https://doi.org/10.1039/c3nr00024a.

[27] F. Furno, K.S. Morley, B. Wong, B.L. Sharp, P.L. Arnold, S.M. Howdle, R. Bayston, P.D. Brown, P.D. Winship, H.J. Reid, Silver nanoparticles and polymeric medical devices: A new approach to prevention of infection?, J. Antimicrob. Chemother. (2004). https://doi.org/10.1093/jac/dkh478.

[28] M.L.W. Knetsch, L.H. Koole, New strategies in the development of antimicrobial coatings: The example of increasing usage of silver and silver nanoparticles, Polymers (Basel). (2011). https://doi.org/10.3390/polym3010340.

[29] N. Durán, P.D. Marcato, G.I.H. De Souza, O.L. Alves, E. Esposito, Antibacterial effect of silver nanoparticles produced by fungal process on textile fabrics and their effluent treatment, J. Biomed. Nanotechnol. (2007). https://doi.org/10.1166/jbn.2007.022.

[30] M.S. Ersoy, E. Onder, Electroless silver coating on glass stitched fabrics for electromagnetic shielding applications, Text. Res. J. (2014). https://doi.org/10.1177/0040517514530025.

[31] A. Taglietti, C.R. Arciola, A. D'Agostino, G. Dacarro, L. Montanaro, D. Campoccia, L. Cucca, M. Vercellino, A. Poggi, P. Pallavicini, L. Visai, Antibiofilm activity of a monolayer of silver nanoparticles anchored to an amino-silanized glass surface, Biomaterials. (2014). https://doi.org/10.1016/j.biomaterials.2013.11.047.

[32] P. Pallavicini, A. Taglietti, G. Dacarro, Y. Antonio Diaz-Fernandez, M. Galli, P. Grisoli, M. Patrini, G. Santucci De Magistris, R. Zanoni, Self-assembled monolayers of silver nanoparticles firmly grafted on glass surfaces: Low Ag+ release for an efficient antibacterial activity, J. Colloid Interface Sci. 350 (2010) 110–116. https://doi.org/10.1016/j.jcis.2010.06.019.

[33] Y. Wan, Z. Guo, X. Jiang, K. Fang, X. Lu, Y. Zhang, N. Gu, Quasi-spherical silver nanoparticles: Aqueous synthesis and size control by the seed-mediated Lee-Meisel method, J. Colloid Interface Sci. 394 (2013) 263–268. https://doi.org/10.1016/j.jcis.2012.12.037.

[34] L. Mandrile, I. Cagnasso, L. Berta, A.M. Giovannozzi, M. Petrozziello, F. Pellegrino, A. Asproudi, F. Durbiano, A.M. Rossi, Direct quantification of sulfur dioxide in wine by Surface Enhanced Raman Spectroscopy, Food Chem. (2020). https://doi.org/10.1016/j.foodchem.2020.127009.

[35] L. Mandrile, M. Vona, A.M. Giovannozzi, J. Salafranca, G. Martra, A.M. Rossi, Migration study of organotin compounds from food packaging by surface-enhanced Raman scattering, Talanta. (2020). https://doi.org/10.1016/j.talanta.2020.121408.

[36] M.D. Abràmoff, P.J. Magalhães, S.J. Ram, Image processing with imageJ,

Biophotonics Int. (2004). https://doi.org/10.1201/9781420005615.ax4.

[37] C. Ortiz, R. Torres, D. Paredes, Synthesis, characterization, and evaluation of antibacterial effect of Ag nanoparticles against Escherichia coli O157:H7 and methicillin- resistant Staphylococcus aureus (MRSA), Int. J. Nanomedicine. (2014) 1717. https://doi.org/10.2147/ijn.s57156.

[38] I. 61851, International Standard International Standard, 61010-1 © Iec2001. 2006 (2006) 13.

[39] F. Quan, A. Mao, M. Ding, S. Ran, J. Wang, G. Yang, Y. Yan, Combustion synthesis and formation mechanism of silver nanoparticles, Int. J. Mater. Res. 109 (2018) 751–755. https://doi.org/10.3139/146.111666.

[40] M. Chen, Y.G. Feng, X. Wang, T.C. Li, J.Y. Zhang, D.J. Qian, Silver nanoparticles capped by oleylamine: Formation, growth, and self-organization, Langmuir. (2007). https://doi.org/10.1021/la700553d.

[41] R.X. He, R. Liang, P. Peng, Y. Norman Zhou, Effect of the size of silver nanoparticles on SERS signal enhancement, J. Nanoparticle Res. (2017). https://doi.org/10.1007/s11051-017-3953-0.

[42] 2007, Performance Standards for Antimicrobial Susceptibility Testing, 2007. https://doi.org/1-56238-525-5.

[43] J.G. Teeguarden, P.M. Hinderliter, G. Orr, B.D. Thrall, J.G. Pounds, Particokinetics in vitro: Dosimetry considerations for in vitro nanoparticle toxicity assessments, Toxicol.

Sci. 95 (2007) 300–312. https://doi.org/10.1093/toxsci/kfl165.

[44] V.M. Ragaseema, S. Unnikrishnan, V. Kalliyana Krishnan, L.K. Krishnan, The antithrombotic and antimicrobial properties of PEG-protected silver nanoparticle coated surfaces, Biomaterials. 33 (2012) 3083–3092. https://doi.org/10.1016/j.biomaterials.2012.01.005.

[45] G. Dacarro, L. Cucca, P. Grisoli, P. Pallavicini, M. Patrini, A. Taglietti, Monolayers of polyethilenimine on flat glass: A versatile platform for cations coordination and nanoparticles grafting in the preparation of antibacterial surfaces, Dalt. Trans. (2012). https://doi.org/10.1039/c1dt11373a.

[46] W. Liu, Y. Wu, C. Wang, H.C. Li, T. Wang, C.Y. Liao, L. Cui, Q.F. Zhou, B. Yan, G.B. Jiang, Impact of silver nanoparticles on human cells: Effect of particle size, Nanotoxicology. (2010). https://doi.org/10.3109/17435390.2010.483745.